PYROCLASTIC DEPOSITS ON MERCURY DETECTED WITH MASCS/MESSENGER DATA: IDENTIFICATION THROUGH SPECTRAL CHARACTERIZATION AND PRINCIPAL COMPONENT ANALYSIS (PCA). A. Galiano[1], F. Capaccioni[1], G. Filacchione[1], C. Carli[1], [1]INAF-IAPS Istituto di Astrofisica e Planetologia Spaziali, Rome, Italy (anna.galiano@inaf.it)

Introduction: The proof of explosive volcanism on Mercury, the innermost planet of the Solar System, is given by the presence of pyroclastic deposits which are characterized by a central pit (vent) surrounded by a bright deposit (facula) showing a steeper spectral slope (increasingly reflectance at longer wavelengths from Ultra-Violet UV to Near-Infrared NIR range) than the average hermean terrain [1,2].

The pyroclastic deposits on Mercury were mainly identified by the analysis of MDIS data (Mercury Dual Imaging System) acquired during the MESSENGER mission, which revealed about 200 of them [2,3,4,5,6,7,8].

Data acquired by MASCS (Mercury Atmospheric and Surface Composition Spectrometer) were used to analyze pyroclastic deposits previously detected with MDIS data [2, 9,10]. Moreover, [11] has employed Principal Component Analysis (PCA) and cluster analysis to detect spectral units on MASCS data acquired during the first and second flybys of MESSENGER without correcting them for viewing geometries.

The present work aims to identify pyroclastic deposits on Mercury by a synergistic approach in which spectral characterization and a PCA are used in sequence on calibrated and photometrically corrected MASCS data acquired during the entire MESSENGER mission.

MASCS data: MASCS' telescope simultaneously feeds an UltraViolet and Visible Spectrometer (UVVS) and a Visible and Infrared Spectrograph (VIRS). VIRS acquired surface reflectance spectra of Mercury in the Visible (VIS, 300-400 nm) and Near Infrared (NIR, 850-1450 nm) range with a spectral sampling of 5 nm [12].

Our analysis involved radiometrically [13] and photometrically [14] corrected VIRS spectra (for incidence and emission angle of 45° and phase angle of 90°) collected from 2011 to 2015. We performed a rigorous selection of the VIRS spectra to achieve optimal observing conditions, therefore characterized by: incidence and emission angles lower than 65°; footprint length lower than 25 km and footprint length/width ratio lower than 10; VIS detector temperature lower than 30 °C, having studied the impact of detector's temperature on the signal's quality through the NESR (Noise-Equivalent Spectral Radiance).

Spectral processing and parameters: The VIS and NIR channels were merged at 0.99 μm and then the Savitsky-Golay (SG) filter was applied to clean the signal from unwanted high-frequency artifacts. Despite the application of the SG filter, the NIR range still shows high oscillations in signal, making it difficult to analyze this spectral range. Starting from these conditions, we have selected the following spectral parameters for our analysis: reflectance at 0.55 μm ($R_{0.55}$), spectral slope in the 0.3-0.4 μm range (UV Slope), spectral slope in the 0.5-0.8 μm range (VIS Slope), crossing wavelength between the extension of UV slope and VIS slope (termed as UV-VIS knee). To minimize remaining photometrical residuals, slopes and knee were estimated on normalized spectra at 0.55 μm.

Spectral characterization of pyroclastic deposits: We used 8 out of 25 IAU catalogued faculae as training fields (Agwo Facula, Amaru Facula, Abeeso Facula, Sarpa Facula, Bibilava Faculae, Orm Faculae, Suge Facula, Nathair Facula). The faculae can be distinguished from the surrounding terrain for the following values of the spectral parameters: $R_{0.55}$ varying between 4% and 12%; UV Slope ranging from 2.7 μm^{-1} to 3.5 μm^{-1}; VIS Slope from 1.6 μm^{-1} to 2.0 μm^{-1}; UV-VIS knee included between 0.42 and 0.52 μm. The spectral characterization of the pyroclastic deposits is coincident with the tail in the $R_{0.55}$ vs. VIS Slope density plot (upper image in Figure 1) and with the secondary cluster and nearby area in the VIS Slope vs. UV Slope density plot (bottom image in Figure 1).

By applying the spectral characterization on VIRS data (filtered for observing angles, footprint, and VIS temperature), the method revealed 50 pyroclastic deposits previously identified [2,3,4], of which 9 of uncertain volcanic nature [5], 18 potential new candidates, and some extended areas with a volcanic origin, i.e. the smooth High-Reflectance Red Plains (HRP) and Intermediate Terrains (IT) located in the North-East, South-West regions of Mercury, and in the floor of Rembrandt crater.

Most faculae are characterized by a UV Slope lower than 3.0 μm^{-1}, whereas Nathair Facula reaches the highest UV Slope value (3.4 μm^{-1}) being responsible for the secondary cluster in the UV Slope vs. VIS slope density plot. Agwo Facula, Abeeso Facula, and an unnamed facula that we term as Facula5, all of them lying on the edge of Caloris Planitia, have UV Slope values intermediate between most of the faculae and Nathair Facula. The reddening of UV Slope can be connected to the lower abundance of iron [15,16] or a finer grain size distribution on those areas [14].

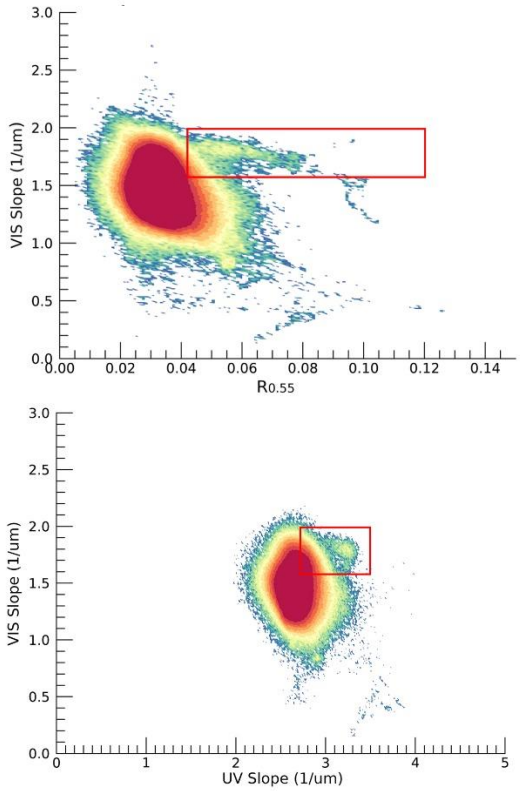

Figure 1: VIS Slope vs $R_{0.55}$ (upper) and VIS Slope vs UV Slope (bottom) density plot of VIRS dataset filtered for observing angles, footprint size, and VIS detector temperature.

Principal Component Analysis (PCA): We used the PCA to reveal spectral units on the Mercury surface and in particular pyroclastic deposits. The PCA was applied on the filtered VIRS dataset as explained above. Furthermore we limited the analysis to the reflectance of 21 channels included between 300 nm and 800 nm sampled at steps of 25 nm. The First three Principal Components (PC1, PC2, PC3) responsible, respectively, for the 98.72%, 0.95%, and 0.17% spectral variability in the dataset. The PC1, PC2, and PC3 appear correlated with the $R_{0.55}$, the VIS Slope, and the UV Slope, respectively.

Pyroclastic deposits, in addition to High-Reflectance Red Plains and Intermediate Terrains, can be mostly distinguished in the map of PC2: they have a lower PC2 value (corresponding to the higher VIS Slope) with respect to other spectral units, such as hollows, which in turn are characterized by a higher PC2 value (coincident to the lower VIS Slope values for the occurrence of a spectral curvature [17]).

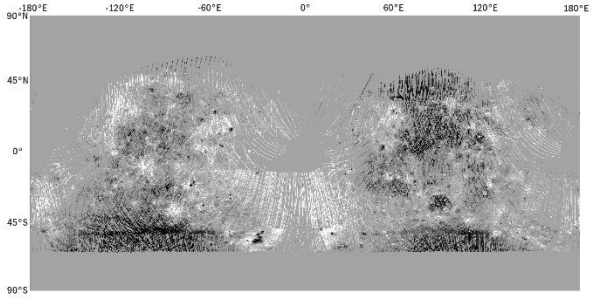

Figure 2: Second Principal Component (PC2) map of Mercury derived from filtered VIRS dataset.

We finally combined the PC1, PC2, and PC3 maps to obtain an RGB image of Mercury surface in cylindrical projection (Figure 2). The PCA RGB maps successfully distinguishes pyroclastic deposits from other minor classes such as hollows, material connected to impact craters (termed as red material), bright crater-floor deposits and fresh crater ejecta, as well as major classes, i.e. Intermediate Terrain (IT) and Low Reflectance Material (LRM) and smooth plains such as High-Reflectance Red Plains (HRP) and Low-Reflectance Blue Plains (LBP).

Acknowledgments: We gratefully acknowledge funding from the Italian Space Agency (ASI) under ASI-INAF agreement 2017-47-H.0.

References: [1] Head J.W. et al. (2008), *Science, 321,* 69-72. [2] Goudge T. A. et al. (2014) *JGR:Planets, 119*, 635-658. [3] Blewett D. et al. (2011) *Science, 333*, 1856-1859. [4] Kerber L. et al. (2011) *PSS, 59*, 1895-1909. [5] Kerber L. et al. (2014) *LPSC XLVII*, Abstract#1777. [6] Thomas R. J. et al. (2014) *JGR:Planets, 119*, 2239-2254. [7] Jozwiak L. M. et al. (2018) *Icarus, 318*, 191-212. [8] Pegg D. L. et al. (2021) *Icarus, 365*, 114510. [9] Besse S. et al. (2020), *JGR:Planets, 125*, e2018JE005879. [10] Barraud O. et al. (2021) *Icarus, 370*, 114652. [11] D'Amore, M. et al. (2011) *LPSC XLII*, Abstract #1608. [12] McClintock W.E. and Lankton, M. R. (2007), *Space Science Rev, 131*, 481-521. [13] Holsclaw, G. M. et al. (2010), *Icarus, 209*, 179-194. [14] Izenberg, N. R. et al. (2014), *Icarus, 228*, 364-374. [15] Rava B. and Hapke B. (1987), *Icarus, 71*, 397-429. [16] Cloutis E. A. et al. (2008), *Icarus 305*, 203-224. [17] Barraud O. et al. (2020), *JGR: Planets, 125*, e2020JE006497.